

Learn Goal-Conditioned Policy with Intrinsic Motivation for Deep Reinforcement Learning

Jinxin Liu^{1,2} Donglin Wang² Qiangxing Tian² Zhengyu Chen²

Abstract

It is of significance for an agent to learn a widely applicable and general-purpose policy that can achieve diverse goals including images and text descriptions. Considering such perceptually-specific goals, the frontier of deep reinforcement learning research is to learn a goal-conditioned policy without hand-crafted rewards. To learn this kind of policy, recent works usually take as the reward the non-parametric distance to a given goal in an explicit embedding space. From a different viewpoint, we propose a novel unsupervised learning approach named goal-conditioned policy with intrinsic motivation (GPIM), which jointly learns both an abstract-level policy and a goal-conditioned policy. The abstract-level policy is conditioned on a latent variable to optimize a discriminator and discovers diverse states that are further rendered into perceptually-specific goals for the goal-conditioned policy. The learned discriminator serves as an intrinsic reward function for the goal-conditioned policy to imitate the trajectory induced by the abstract-level policy. Experiments on various robotic tasks demonstrate the effectiveness and efficiency of our proposed GPIM method which substantially outperforms prior techniques.

1. Introduction

Reinforcement learning (RL) makes it possible to drive agents to achieve sophisticated goals in complex and uncertain environments, from computer games (Badia et al., 2020; Berner et al., 2019) to real robot control (Lee et al., 2018; Lowrey et al., 2018; Vecerik et al., 2019; Popov et al., 2017), which usually involves learning a specific policy for individual task relying on task-specific reward. However, autonomous agents are expected to exist persistently in the world and have the ability to solve diverse tasks. To achieve

this, one needs to build a universal reward function and design a mechanism to spontaneously generate diverse goals for training. Raw sensory inputs such as images have been considered as common goals for agents to practice on and achieve (Watter et al., 2015; Florensa et al., 2019; Nair et al., 2018; 2019), which further exacerbates the challenge for designing autonomous RL agents that can deal with such perceptually-specific inputs.

Previous works make full use of a goal-achievement reward function as available prior knowledge (Pong et al., 2018), such as Euclidean distance. Unfortunately, this kind of measurement in the original space is not very effective for visual tasks since the distance between images does not correspond to a meaningful distance between states (Zhang et al., 2018). Further, the measure function is applied in the embedding space, where the representations of raw sensory inputs are learned by means of using a latent variable model like VAE (Higgins et al., 2017b; Nair et al., 2018) or using the contrastive loss (Sermanet et al., 2018; Warde-Farley et al., 2019). We argue that these approaches taking a prior non-parametric reward function in the original or embedding space as above may limit the repertoires of behaviors and impose manual engineering burdens (Pong et al., 2019).

In the absence of any prior knowledge about the measure function, standard unsupervised RL methods learn a *latent-conditioned policy* through the lens of empowerment (Salge et al., 2014; Eysenbach et al., 2018; Sharma et al., 2019) or the self-consistent trajectory autoencoder (Co-Reyes et al., 2018; Hausman et al., 2018). However, such a learned policy is conditioned on the latent variables rather than perceptually-specific goals. Applying these procedures to goal-reaching tasks, similar to parameter initialization or the hierarchical RL, needs an external reward function for the new tasks; otherwise the learned latent-conditioned policy cannot be applied directly to user-specified goals.

Different from previous work, a novel unsupervised RL scheme is proposed in this paper to learn a goal-conditioned policy by jointly learning an extra abstract-level policy conditioned on latent variables. The abstract-level policy is trained to generate *diverse abstract skills* while the goal-conditioned policy is trained to efficiently achieve perceptually-specific goals that are rendered from the states

¹Zhejiang University ²Westlake University. Correspondence to: Donglin Wang <wangdonglin@westlake.edu.cn>.

Project site: <https://sites.google.com/view/gpim>

induced by the corresponding abstract skills. Specifically, we optimize a discriminator in an unsupervised manner for the purpose of reliable exploration (Salge et al., 2014) to provide the intrinsic reward for the abstract-level policy. Then the learned discriminator serves as an intrinsic reward function for the goal-conditioned policy to imitate the trajectory induced by the abstract-level policy. In essence, *the abstract-level policy can reproducibly influence the environment, and the goal-conditioned policy perceptibly imitates these influences*. It is worth noting that both the abstract-level and goal-conditioned policies share an identical intrinsic reward function which is learned only at the abstract level. This procedure enables the latent-conditioned intrinsic reward as a proxy to reward the goal-conditioned policy for various perceptually-specific goals. As opposed to directly scoring the current states with regards to the goals, we obtain the reward by matching the goals with the associated latent variables, which gets benefit from the discriminator.

The main contribution of our work is an unsupervised RL method that can learn a perceptually-specific goal-conditioned policy via the intrinsic reward. Our training procedure explicitly decouples the reward learning process and policy optimization, which makes the obtained reward function universal and effective for various perceptual goals, including images and text descriptions. Furthermore, we show that our intrinsic reward holds a well-shaped embodiment in terms of the training environment dynamics, and as a result benefits the training efficiency on extensive goal-reaching tasks.

2. Preliminaries

Reinforcement Learning: An agent interacts with an environment and selects actions in reinforcement learning (RL) so as to maximize the expected amount of reward received in the long run (Sutton & Barto, 2018), which can be modeled as a Markov decision process (MDP) (Puterman, 2014). An MDP is defined as a tuple $\mathcal{M} = (S, A, p, R, \gamma)$, where S and A are state and action spaces, $p(\cdot|s, a)$ gives the next-state distribution upon taking action a in state s , $R(s, a, s')$ is a random variable representing the reward received at transition $s \xrightarrow{a} s'$, and $\gamma \in [0, 1)$ is a discount factor.

Intrinsic Motivation: RL with intrinsic motivation typically focuses on abstracting actions or exploring the environment, by maximizing the empowerment (Achiam et al., 2018; Salge et al., 2014), or encouraging novelty-seeking states based on the model uncertainty (Pathak et al., 2019; Still & Precup, 2011) or the model prediction error (Burda et al., 2019; Pathak et al., 2017; Oudeyer et al., 2007). Here, we promote reproducible skills by maximizing the empowerment to acquire the intrinsic reward, guiding the emergence of the goal-conditioned policy. Specifically, the uniform objective is to maximize the mutual information between latent

variables ω and agent’s behaviors τ : $\mathcal{I}(\omega; \tau)$, where the specific manifestation of τ can be an entire trajectory (Achiam et al., 2018), an individual state (Eysenbach et al., 2018) or a final state (Gregor et al., 2016). The specific implementation includes *reverse* and *forward* two forms (Campos et al., 2020). Please refer to Aubret et al. (2019) for more details.

3. The Method

In this section, we first formalize the problem and introduce the framework. Second, we elaborate on the process of how to jointly learn the goal-conditioned policy and abstract-level policy. Third, we apply the latent variable models in our setting to improve the generalization ability.

3.1. Overview

Given perceptually-specific goals g , our objective is to learn a goal-conditioned policy $\pi_\theta(a|\tilde{s}, g)$ that inputs state \tilde{s} and g and outputs action a as shown in Figure 1. The abstract-level policy $\pi_\mu(a|s, \omega)$ takes as input a state s and a latent variable ω and outputs action a , where ω corresponds to diverse latent skills. The discriminator q_ϕ is firstly trained at the abstract-level for reliable exploration, and then it provides the reward signal for the goal-conditioned policy to imitate the trajectory induced by the abstract-level policy. Critically, the abstract-level policy is able to generate diverse states s that are further rendered as diverse perceptually-specific goals $g = \text{Render}(s)$, where the *Render* is similar in spirit to the social partner in Colas et al. (2020). On this basis, $\pi_\theta(a|\tilde{s}, g)$ conditioned on the rendered goal g interacts with the reset environment under the instruction of the reward function q_ϕ . We use the non-tilde s and the tilde \tilde{s} to distinguish between the states of two policies respectively. Actually, \tilde{s} and s come from the same state space.

3.2. Proposed GPIM Method

In order to jointly learn the abstract-level policy $\pi_\mu(a|s, \omega)$ and goal-conditioned policy $\pi_\theta(a|\tilde{s}, g)$, we maximize the mutual information between the state s and latent variable ω for π_μ , and simultaneously maximize the mutual information between the state \tilde{s} and goal g for π_θ . Consequently, the overall objective function to be maximized can be expressed as follows¹

$$\mathcal{F}(\mu, \theta) = \mathcal{I}(s; \omega) + \mathcal{I}(\tilde{s}; g). \quad (1)$$

For clarification, Figure 2 depicts the graphical model for the latent variable ω , state s induced by π_μ , goal g rendered from s , and state \tilde{s} induced by π_θ . As seen, the latent

¹To further clarify the motivation, we conduct the ablation study to compare our method with that just maximizing $\mathcal{I}(s; \omega)$ and that just maximizing $\mathcal{I}(s; g)$ in Appendix A.1.

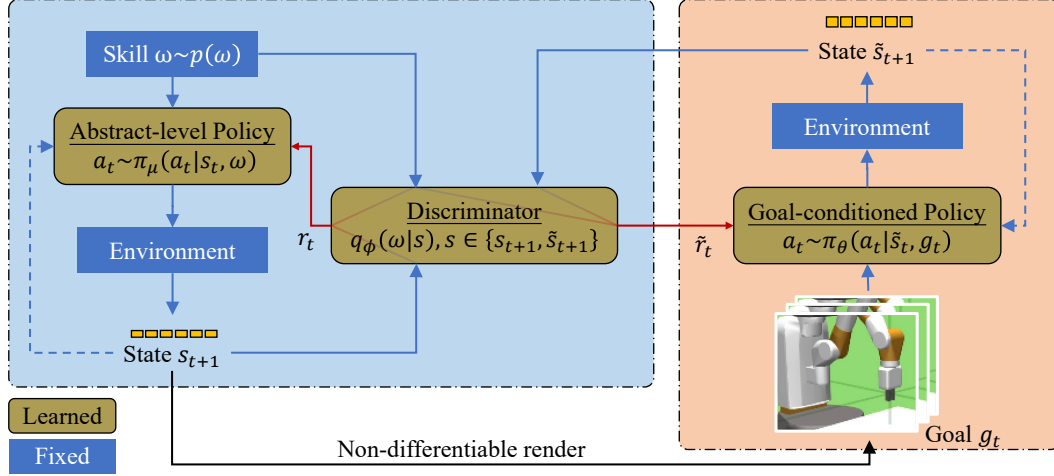


Figure 1. Framework of GPIM. We jointly train the abstract-level policy π_μ and the discriminator q_ϕ to understand skills which specify task objectives (e.g., trajectories, the final goal state), and use such understanding to reward the goal-conditioned policy for completing such tasks (rendered goals). State s_{t+1} (e.g., position of an agent) induced by π_μ is converted into a perceptually-specific goal g_t (e.g., image showing the position of the agent) for π_θ . Note that the two environments in the figure are identical, and the initial states s_0 of π_μ and \tilde{s}_0 of π_θ are sampled from the same distribution.

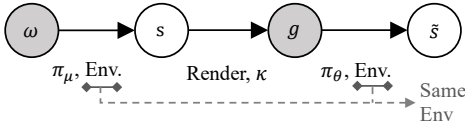


Figure 2. Graphical model: abstract-level policy π_μ provides goals and the associated reward for the goal-conditioned policy π_θ .

variable $\omega \sim p(\omega)$ ² is firstly used to generate state s via the policy π_μ interacting with the environment. Then, we use the state s to generate perceptually-specific goal g . After that, the goal-conditioned policy π_θ outputs action a to interact with the environment to obtain the state \tilde{s} at the next time step. In particular, ω is expected to generate diverse behavior modes through π_μ while π_θ behaving like \tilde{s} is to imitate this behavior by taking as input the rendered goal g .

Based on the context, the correlation between \tilde{s} and g is no less than that between \tilde{s} and w , so that $\mathcal{I}(\tilde{s}; g) \geq \mathcal{I}(\tilde{s}; \omega)$ (Beaudry & Renner, 2011). Thus, we can obtain the lower bound of $\mathcal{F}(\mu, \theta)$:

$$\begin{aligned} \mathcal{F}(\mu, \theta) &\geq \mathcal{I}(s; \omega) + \mathcal{I}(\tilde{s}; \omega) \\ &= \mathcal{H}(\omega) - \mathcal{H}(\omega | s) + \mathcal{H}(\omega) - \mathcal{H}(\omega | \tilde{s}) \quad (2) \\ &= 2\mathcal{H}(\omega) + \mathbb{E}_{p_m(\cdot)} [\log p(\omega | s) + \log p(\omega | \tilde{s})], \end{aligned}$$

where $p_m(\cdot) \triangleq p(\omega, s, g, \tilde{s}; \mu, \kappa, \theta)$ denotes the joint distribution of ω, s, g and \tilde{s} specified by the graphic model in Figure 2, and κ refers the Render. Since it is difficult to ex-

² $p(\omega)$ denotes the prior distribution. Fixing $p(\omega)$ instead of learning it is to prevent π_μ from collapsing to sampling only a handful of skills. In experiment, we use a categorical distribution for $p(\omega)$ following DIAYN (Eysenbach et al., 2018).

actly compute the posterior distributions $p(\omega | s)$ and $p(\omega | \tilde{s})$, Jensen’s Inequality (Barber & Agakov, 2003) is further applied for approximation by using a learned discriminator network $q_\phi(\omega | \cdot)$ (see Appendix B.1 for the derivation). Thus, $\mathcal{F}(\mu, \theta) \geq \mathcal{J}(\mu, \phi, \theta)$, where

$$\mathcal{J}(\mu, \phi, \theta) \triangleq 2\mathcal{H}(\omega) + \mathbb{E}_{p_m(\cdot)} [\log q_\phi(\omega | s) + \log q_\phi(\omega | \tilde{s})].$$

It is worth noting that the identical discriminator q_ϕ with the parameter ϕ is used for the variational approximation of $p(\omega | s)$ and $p(\omega | \tilde{s})$. For the state s induced by skill w and \tilde{s} originating from g , the shared discriminator q_ϕ assigns a similarly high probability on w for both states s and \tilde{s} associated with the same ω . Intuitively, we factorize acquiring the goal-conditioned policy π_θ and learn it purely in the space of the agent’s embodiment (i.e., the latent ω) — separate from the perceptually-specified goals (e.g., images and text descriptions), where goals in these two spaces (ω and perceptual goals g) have different characteristics due to the underlying manifold spaces. Therefore, q_ϕ can be regarded as a reward network shared by the abstract-level policy $\pi_\mu(a | s, \omega)$ and goal-conditioned policy $\pi_\theta(a | \tilde{s}, g)$.

According to the objective function $\mathcal{J}(\mu, \phi, \theta)$, we propose an alternating optimization between π_μ and π_θ as follows:

Step I: Fix π_θ and update π_μ and q_ϕ . In this case, θ is not a variable to update and $\mathcal{J}(\mu, \phi, \theta)$ becomes

$$\begin{aligned} \mathcal{J}(\mu, \phi) &= \mathbb{E}_{p(\omega, s; \mu)} [\log q_\phi(\omega | s)] \\ &\quad + \underbrace{\mathbb{E}_{p_m(\cdot)} [\log q_\phi(\omega | \tilde{s}) - 2 \log p(\omega)]}_{\text{Variable independent term}}. \quad (3) \end{aligned}$$

According to Equation 3, $\mathcal{J}(\mu, \phi)$ can be thus optimized by

Algorithm 1 Learning process of our proposed GPIM

```

1: while not converged do
2:   Sample skill:  $\omega \sim p(\omega)$ .
3:   # Step I:  $\pi_\mu$  renders goals, and learns rewards for  $\pi_\theta$ .
4:   Sample initial state:  $s_0 \sim p_0(s)$ .
5:   for  $t = 0, 1, \dots, T$  steps do
6:     Sample action:  $a_t \sim \pi_\mu(a_t|s_t, \omega)$ .
7:     Step environment:  $s_{t+1} \sim p(s_{t+1}|s_t, a_t)$ .
8:     Render:  $g_t = \text{Render}(s_{t+1})$ .  $\triangleright$  Record goals.
9:     Compute reward  $r_t$  for policy  $\pi_\mu$  using (4).
10:    Update policy  $\pi_\mu$  to maximize  $r_t$  with SAC.
11:    Update discriminator ( $q_\phi$ ) to maximize
         $\log q_\phi(\omega|s_{t+1})$  with SGD.
12:   end for
13:   # Step II:  $\pi_\theta$  imitates  $\pi_\mu$  with the rendered goals and
        the associated rewards (for the same  $\omega$ ).
14:   Sample initial state:  $\tilde{s}_0 \sim p_0(\tilde{s})$ .
15:   for  $t = 0, 1, \dots, T$  steps do
16:     Recap dynamic goal  $g_t$  from the recorded goals.
        # Note:  $g_t = g_T$  for fixed goals.
17:     Sample action:  $a_t \sim \pi_\theta(a_t|\tilde{s}_t, g_t)$ .
18:     Step environment:  $\tilde{s}_{t+1} \sim p(\tilde{s}_{t+1}|\tilde{s}_t, a_t)$ .
19:     Compute reward  $\tilde{r}_t$  for policy  $\pi_\theta$  using (6).
20:     Update policy  $\pi_\theta$  to maximize  $\tilde{r}_t$  with SAC.
21:   end for
22: end while
    
```

setting the intrinsic reward at time step t for π_μ as

$$r_t = \log q_\phi(\omega|s_{t+1}) - \log p(\omega), \quad (4)$$

where the term $-\log p(\omega)$ is added for agents to avoid artificial termination and reward-hacking issues (Amodi et al., 2016). We implement this optimization with soft actor-critic (SAC). On the other hand, the reward network q_ϕ can be updated with SGD by maximizing $\mathbb{E}_{p(\omega, s; \mu)} [\log q_\phi(\omega|s)]$.

Step II: Fix π_μ and q_ϕ to update π_θ . In this case, μ and ϕ are not variables to update any more and $\mathcal{J}(\mu, \phi, \theta)$ can be simplified as

$$\begin{aligned} \mathcal{J}(\theta) = & \mathbb{E}_{p_m(\cdot)} [\log q_\phi(\omega|\tilde{s})] \\ & + \underbrace{\mathbb{E}_{p(\omega, s; \mu)} [\log q_\phi(\omega|s) - 2 \log p(\omega)]}_{\text{Variable independent term}}. \end{aligned} \quad (5)$$

According to Equation 5, $\mathcal{J}(\theta)$ can thus be optimized by setting the intrinsic reward at time step t for π_θ as

$$\tilde{r}_t = \log q_\phi(\omega|\tilde{s}_{t+1}) - \log p(\omega), \quad (6)$$

where the term $-\log p(\omega)$ is added for the same reason as above and we also implement this optimization with SAC.

These two steps are performed alternately until convergence. In summary, we train the goal-conditioned policy π_θ along with an extra abstract-level policy π_μ by using a procedural render, which explicitly decouples the procedure of unsupervised RL into the generation of goals and the associated reward function, and the training of goal-conditioned policy. The overall procedure of our proposed GPIM is summarized in Algorithm 1.

Implementing π_θ with latent variable models: As indicated by Srinivas et al. (2020), agent’s control algorithms built on top of useful semantic representations are required to be data-efficient. For this purpose, our goal-conditioned policy π_θ is specifically implemented by considering an additional *regularization loss* on the perception

level (Hafner et al., 2020; Tanwani, 2020) to improve the learning efficiency and generalization when facing with high-dimensional perceptually-specific goals. More concretely, we incorporate a latent variable model (Kingma & Welling, 2013; Higgins et al., 2017a) into the specific implementation of goal-conditioned policy π_θ , where we use the extracted latent representation of goals in the training procedure. One can see Appendix A.2 for more details. Furthermore, we conduct additional experiments to demonstrate that such regularization loss is important to improve learning efficiency and generalization ability of our goal-conditioned policy.

4. Analysis

Normally, unsupervised RL seeks the goal-conditioned policy $\pi_\theta(a|\tilde{s}, g)$ that maximizes $\mathcal{I}(g; \tilde{s})$, while our GPIM learns $\pi_\theta(a|\tilde{s}, g)$ by maximizing $\mathcal{I}(s; \omega) + \mathcal{I}(\tilde{s}; g)$. Here we characterize the theoretical connection of learned policies between the two objectives.

Let $\eta(\pi_\theta) \triangleq \mathcal{I}(g; \tilde{s}) = \mathbb{E}_{p(g, \tilde{s}; \theta)} [\log p(g|\tilde{s}) - \log p(g)]$, and $\hat{\eta}(\pi_\theta) = \mathbb{E}_{p(\omega, s, g, \tilde{s}; \mu, \kappa, \theta)} [\log p(\omega|\tilde{s}) - \log p(\omega)]$ subject to $\mathcal{I}(\omega; s) \geq C$. For brevity, we first assume the prior goal distribution $p(g)$ for optimizing $\eta(\pi_\theta)$ matches the goal distribution $p(g|\omega; \mu, \kappa)$ induced by π_μ and render κ for optimizing $\hat{\eta}(\pi_\theta)$. We arrive at (recalling $\omega \xrightarrow{\mu} s \xrightarrow{\kappa} g \xrightarrow{\theta} \tilde{s}$):

$$\begin{aligned} \hat{\eta}(\pi_\theta) - \eta(\pi_\theta) & \quad \# p_m(\cdot) \triangleq p(\omega, s, g, \tilde{s}; \mu, \kappa, \theta) \\ & \approx \mathbb{E}_{p_m(\cdot)} [\log p(\omega|\tilde{s}) - \log p(\omega) - \log p(g|\tilde{s}) + \log p(g)] \\ & = \mathbb{E}_{p_m(\cdot)} [\log p(\tilde{s}|\omega; \mu, \kappa, \theta) - \log p(\tilde{s}|g; \theta)] \\ & = \mathbb{E}_{p(\omega, s, g; \mu, \kappa)} [\log p(s|\omega; \mu) + \log p(g|s; \kappa)] \end{aligned} \quad (7)$$

Equation 7 comes from the graphic model in Figure 2, specifying that $p(\tilde{s}|\omega; \mu, \kappa, \theta) = p(s|\omega; \mu)p(g|s; \kappa)p(\tilde{s}|g; \theta)$, where $p(s|\omega; \mu)$ and $p(g|s; \kappa)$ refer to the interaction of π_μ and the render procedure, respectively. Ignoring the

render term $p(g|s; \kappa)$, we have $0 \geq \hat{\eta}(\pi_\theta) - \eta(\pi_\theta) \approx -\mathcal{H}(s|\omega) \geq C - \mathcal{H}(s)$. The former " \geq " denotes that our $\hat{\eta}(\pi_\theta)$ lower bounds the standard objective $\eta(\pi_\theta)$. The latter " \geq " shows that this bound becomes tight as the auxiliary $\mathcal{I}(\omega, s)$ approaches $\mathcal{H}(s)$ (larger C). Furthermore, if the induced goal distribution $p(\omega)p(g|\omega; \mu, \kappa)$ does not match the prior $p(g)$ for maximizing $\eta(\pi_\theta)$, we can derive $\hat{\eta}(\pi_\theta) - \eta(\pi_\theta) \leq 2R_{max}\sqrt{\epsilon/2}$, where R_{max} refers the maximum reward $\log p(g|\tilde{s}) - \log p(g)$ over $p(g)(\tilde{s}|g; \theta)$, and $\epsilon = \mathbb{E}_{p(\omega, s; \mu)} [D_{KL}(p(g, s|\omega, s; \kappa, \theta) \| p(g, s; \theta))]$. Please see Appendix B.2 for a full derivation.

5. Related Work

Investigating the goal distribution: For goal-reaching tasks, many prior methods (Schaul et al., 2015; Andrychowicz et al., 2017; Levy et al., 2017; Pong et al., 2018; Hartikainen et al., 2019) assume an available distribution of goals during exploration. In the unsupervised RL setting, the agent needs to automatically explore the environment and discover potential goals, which is critical for learning a universal goal-conditioned policy. The setting of discovering goals for the policy has been discussed in Baranes & Oudeyer (2013), which introduces the self-adaptive goal generation architecture to motivate goal exploration. Recently, several works (Colas et al., 2018; Warde-Farley et al., 2019; Florensa et al., 2019; Kovač et al., 2020; Nair et al., 2018; Péré et al., 2018; Pong et al., 2019) adopt heuristics to acquire a goal distribution based on previously visited states.

Learning the goal-achievement reward function: Building on prior works in standard RL algorithms (Schaul et al., 2015; Schulman et al., 2017; Haarnoja et al., 2018) to learn policies with prior goals and rewards, unsupervised RL faces another challenge — automatically learning the goal-achievement reward function. Two common approaches to obtain rewards are (1) applying the *pre-defined function* on the learned goal representations, and (2) *directly learning a reward function*. Estimating the reward with the *pre-defined function* typically adopts self-supervised algorithms to acquire the representation: Warde-Farley et al. (2019) performs maximum likelihood estimation to represent goals, several works (Nair et al., 2018; Florensa et al., 2019; Nair et al., 2019; Pong et al., 2019; Pitis et al., 2020) elicit the goal representation with VAE, and Sermanet et al. (2018) employs contrastive learning to acquire effective perception for high-dimensional inputs. Over the learned representations, this approach applies a prior non-parametric measure function (e.g., the cosine similarity) to provide rewards. This contrasts with our decoupled training procedure, where we acquire the reward by matching current states with their associated latent variables, instead of the perceptual goals. This provides more flexibility in training the policy than using an embedding-based reward, especially faced with

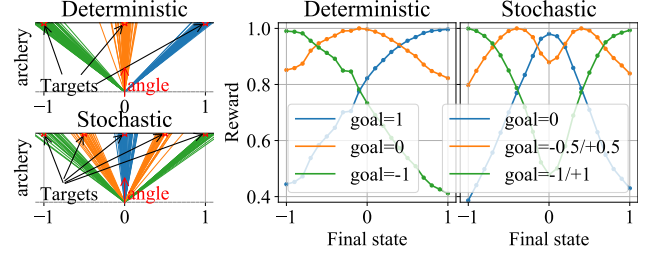


Figure 3. "Archery" tasks and the learned rewards on both deterministic and stochastic environments.

heterogeneous states and goals.

Another approach, *directly learning a reward function*, aims at pursuing skills (the latent-conditioned policy) by maximizing the empowerment (Salge et al., 2014), which draws a connection between option discovery and information theory. This procedure (Achiam et al., 2018; Eysenbach et al., 2018; Gregor et al., 2016; Campos et al., 2020; Sharma et al., 2019; Tian et al., 2020) typically maximizes the mutual information between a latent variable and the induced behaviors (states or trajectories), which is optimized by introducing a latent-conditioned reward function. While capable of learning a latent-conditioned policy, it is difficult to apply the latent-conditioned reward to guiding the policy to pursue user-specified perceptually-specific goals. Our approach explicitly decouples latent-conditioned reward learning and goal-conditioned policy learning, suggesting the effectiveness of the latent-conditioned reward on accounting for the perceptually-specific goals.

Hindsight, self-play and knowledge distillation: Our method is similar in spirit to goal relabeling methods like hindsight experience replay (HER) (Andrychowicz et al., 2017) which replays each episode with a different goal in addition to the one the agent was trying to achieve. However, HER requires a prior reward function and a hand-crafted goal space. By contrast, our proposed GPIM is unsupervised and able to find its own goal space. The self-play (Sukhbaatar et al., 2017; 2018) is closely related to our scheme, leading to emergent autocurricula by pitting two versions of the same agent against one another. However, these approaches generally require prior reward functions. As for knowledge distillation (Xu et al., 2020), we aim at extracting the relationship between two different tasks.

6. Experiments

Extensive experiments are conducted to evaluate our proposed GPIM method, where the following four questions³ will be considered in the main paper: 1) By using the "archery" task, we clarify whether q_ϕ can provide an ef-

³Due to the page limitation, more experimental analysis and results are included in the Appendix.

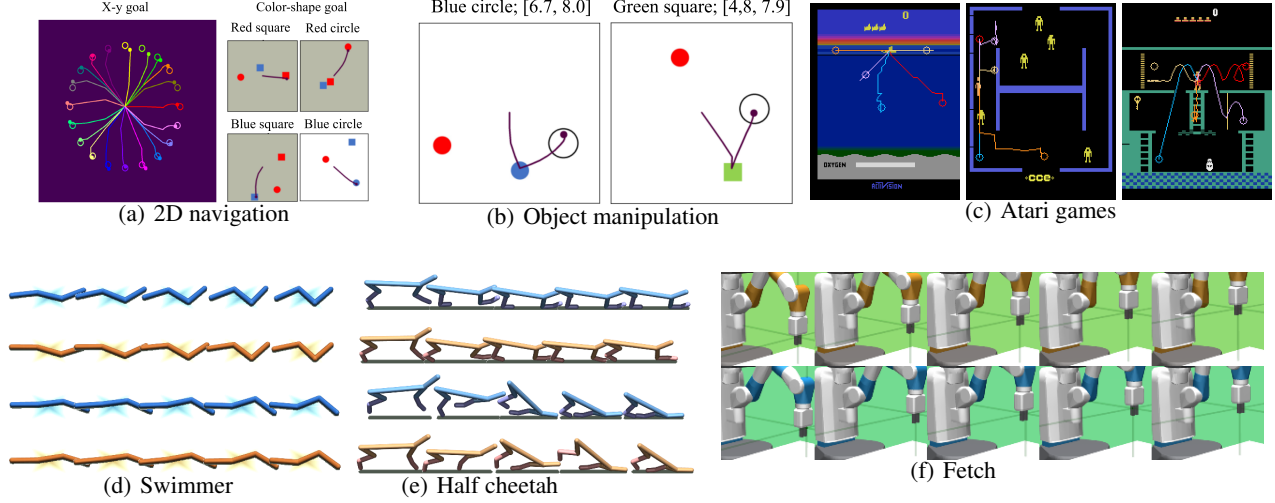


Figure 4. Goals and learned behaviors by GPIM: Dots in 2D navigation (left subfigure, x - y goal) and atari games denote different final goal states, and curves with same color represent corresponding trajectories; Goals in 2D navigation (right subfigure, color-shape goal) and object manipulation are described using the text at the top of the diagram, where the purple lines imply the behaviors; In mujoco tasks, the first (swimmer, half cheetah and fetch) and third (swimmer and half cheetah) rows represent the expert trajectories, and each row below represents the corresponding behavior.

fective reward function on learning the goal-conditioned policy π_θ . Furthermore, more complex tasks including navigation, object manipulation, atari games, and mujoco tasks are introduced to answer: 2) Does our model learn effective behaviors conditioned on a variety of goals, including high-dimensional images and text descriptions that are heterogeneous to states? 3) Does the proposed GPIM on learning a goal-conditioned policy outperform baselines? 4) Does the learned reward function produce better expressiveness of tasks, compared with the prior non-parametric function in the embedding space? Video is available under <https://sites.google.com/view/gpim>.

Visualizing the learned reward function. We start with simple "archery" task to visualize how the learned reward function (discriminator q_ϕ) accounts for goal-conditioned behaviors in dynamics. The task shown in Figure 3 requires choosing an angle at which we shoot an arrow to the target. The left upper subfigure shows that in a deterministic environment, given three different but fixed targets (with different colors), the arrow reaches the corresponding target successfully under the learned reward function q_ϕ . The reward as a function of the final location of arrows in three tasks is shown on the right. We can find that the learned reward functions resemble convex in terms of the distance between final states to targets, where vertexes appear in the positions of the corresponding targets. Specifically, the maximum value of the learned reward function is achieved when the final state is close to the given target. The farther away the agent's final state is from the target, the smaller this reward value is. Similarly, the same conclusion can

be drawn from the stochastic environment in the left lower subfigure, where the angle of the arrow has a 50% chance to become a mirror-symmetric angle. We see that the learned reward function substantially describes the dynamics and the corresponding tasks, both in deterministic and stochastic environments. This answers our *first* question.

Scaling to more complex tasks. To answer our *second* question, we now consider more complex tasks as shown in Figure 4. 1) In *2D navigation tasks*, an agent can move in each of the four cardinal directions. We consider the following two tasks: moving the agent to a specific coordinate named x - y goal⁴ and moving the agent to a specific object with certain color and shape named *color-shape goal*. 2) *Object manipulation* considers a moving agent in 2D environment with one block for manipulation, and the other block as a distractor. The agent first needs to reach the block and then move the block to the target location, where the block is described using color and shape. In other words, the description of the goal contains the *color-shape goal* of the true block and the x - y goal of the target coordinate. 3) Three *atari games* including seaquest, berzerk and montezuma revenge require an agent to reach the given final states. 4) We use three *mujoco tasks* (swimmer, half cheetah, and fetch) taken from OpenAI GYM (Brockman et al., 2016) to fast imitate given expert trajectories. Specifically, the goals for π_θ in 2D navigation, object manipulation and atari games are the rendered final state s_T induced by abstract-

⁴Definitions of x - y goal, *color-shape goal*, and environment details are given in Appendix C.1.

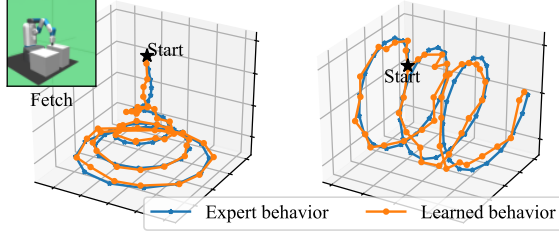


Figure 5. Expert behaviors and learned behaviors on Fetch task.

level policy π_μ : $g_t = \text{Render}(s_T)$, and the goals for π_θ in mujoco tasks are the rendered trajectories induced by π_μ : $\{g_0, g_1, \dots\} = \text{Render}(\{s_1, s_2, \dots\})$.

The left subfigure of Figure 4(a) shows the learned behaviors of navigation in continuous action space given the x-y goal which is denoted as the small circle, and the right subfigure shows the trajectory of behavior with the given color-shape goal. More results on discrete navigation can be found in Appendix E. As observed, the agent manages to learn navigation tasks by using GPIM. Further, 2D navigation with color-shape goal (Figure 4(a) right) and object manipulation tasks (Figure 4(b)) show the effectiveness of our model facing heterogeneous goals and states. Specifically, Figure 4(b) shows the behaviors of the agent on object manipulation, where the agent is asked to first arrive at a block (i.e., blue circle and green square respectively) and then push it to the target location inside a dark circle (i.e., [6.7, 8.0] and [4.8, 7.9] respectively), where the red object exists as a distractor. Figure 4(c) shows the behaviors of agents that reach the final states in a higher dimensional (action, state and goal) space on *sequest*, *berzerk* and *montezuma revenge* respectively. Figure 4(d-f) shows how the agent imitates expert trajectories of *swimmer*, *half cheetah* and *fetch*.

By learning to reach diverse goals generated by the abstract-level policy and employing the regularization loss to represent the goals, the agent learns the ability to infer new goals later encountered by the agent. For example, as in Figure 4(a) (right), learning three behaviors with the goal of red-square, red-circle or blue-square in a gray background makes the agent accomplish the new goal of blue-circle in a white background. We further conduct the ablation study in Appendix A.2 to show how the regularization loss affects the learned behaviors, and use more experiments to show the generalization of the goal-conditioned policy to unseen goals in Appendix A.3.

Considering the time-varying rendered goals in *fetch task*, we further demonstrate the ability of GPIM on temporally-extended tasks, where the gripper of the robotic arm is used to render a series of 3D coordinates as goals for imitation in the training phase. We make agents imitate the given composite behaviors (i.e., expert behaviors) and show their per-

formance in Figure 5. During test, we employ two parameterized complex curves for the gripper to follow: $(x, y, z) = (t \sin(t)/50, t \cos(t)/50 - 1/50, -\log(t+1)/5)$ (left), and $(x, y, z) = (t/5, \cos(t)/5 - 1/5, \sin(t)/5)$ (right). It is worth noting that during training the agent is required to imitate a large number of simple behaviors and has never seen such complex goals before testing. It is observed from Figure 5 that the imitation curves are almost overlapping with the given expert trajectories, indicating that the agent using GPIM framework has the potential to learn such compositional structure of goals during training and generalize to new composite goals during test.

Comparison with baselines. For the *third* question, we compare our method to three baselines: **RIG** (Nair et al., 2018), **DISCERN** (Warde-Farley et al., 2019), and **L2 Distance**. L2 Distance measures the distance between states and goals, where the L2 distance $-||s_t - s_g||^2 / \sigma_{\text{pixel}}$ is considered with a hyperparameter σ_{pixel} . Note that 2D navigation with the color-shape goal and object manipulation using text description makes the dimensions of states and goals different, so L2 cannot be used in these two tasks. In RIG, we obtain rewards by using the distances in two embedding spaces and learning two independent VAEs, where one VAE is to encode states and the other is to encode goals. We use the normalized distance to goals⁵ as the evaluation metric, where we generate 50 goals (tasks) as validation.

We show the results in Figure 6 by plotting the normalized distance to goals as a function of the number of actor’s steps, where each curve considers 95% confidence interval in terms of the mean value across three seeds. As observed, our GPIM consistently outperforms baselines in almost all tasks except for the RIG in 2D navigation (x-y goal) due to the simplicity of this task. Particularly, as the task complexity increases from 2D navigation (x-y goal) to 2D navigation (color-shape goal) and eventually object manipulation (mixed x-y goal and color-shape goal), GPIM converges faster than baselines and the performance gap between our GPIM and baselines becomes larger. Moreover, although RIG learns fast on navigation with x-y goal, it fails to accomplish complex navigation with color-shape goal because the embedding distance between two independent VAEs has difficulty in capturing the correlation of heterogeneous states and goals. Especially in high-dimensional action space and on more exploratory tasks (atari and mujoco tasks), our method substantially outperforms the baselines.

To gain more intuition for our method, we record the distance (Δr) between the final state induced by π_θ and the goal rendered by π_μ throughout the training process of the 2D navigation (x-y goal). In this specific experiment, we update π_μ and q_ϕ but ignore the update of π_θ before 200 k

⁵Definition and further descriptions can be found in Appendix C.2.

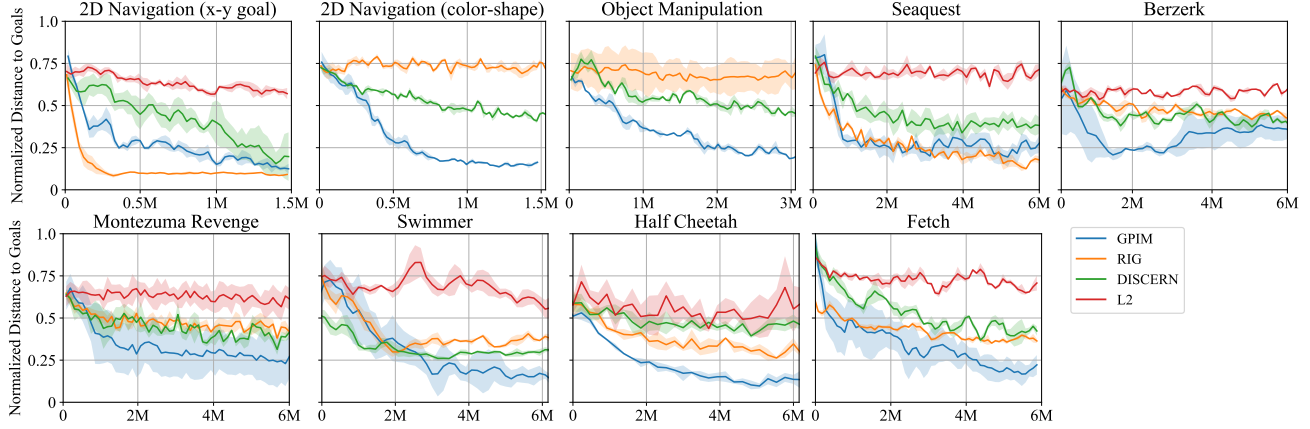


Figure 6. Performance (normalized distance to goals vs. actor steps) of our GPIM model and three baselines (RIG, DISCERN and L2).

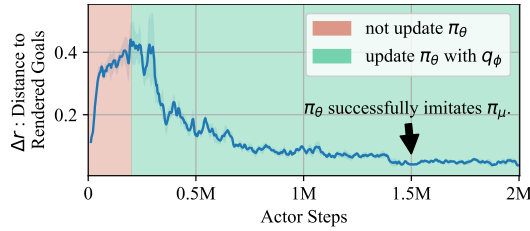


Figure 7. The abstract-level policy π_μ gradually explores the environment, generating more difficult goals. Then the learned reward function q_ϕ encourages π_θ to gradually mimic π_μ .

steps to show the exploration of π_μ at the abstract level. As shown in Figure 7, Δr steadily increases during the first 200 k steps, indicating that the abstract-level policy π_μ explores the environment (i.e., goal space) to distinguish skills more easily, and as a result, generates diverse goals for training the goal-conditioned policy π_θ . After around 1.5 M training steps, Δr almost comes to 0, indicating that the goal-conditioned policy π_θ has learned a good strategy to reach the rendered goals. In Appendix A.4, we visually show the generated goals at the abstract level in more complex tasks, which shows that our straightforward framework can effectively explore the environment without additional sophisticated exploration strategies.

Expressiveness of the reward function. Particularly, the performance of unsupervised RL methods depends on the diversity of autonomously generated goals and the expressiveness of the learned reward function, which is conditioned on the generated goals. We have shown that our straightforward framework can effectively explore the environment. The next question is that: with the same exploration capability to generate goals for training, does our model achieve competitive performance against the baselines? Said another way, will the obtained reward (over embedding space) of baselines taking the prior non-parametric function limit the repertoires of learning tasks in a specific

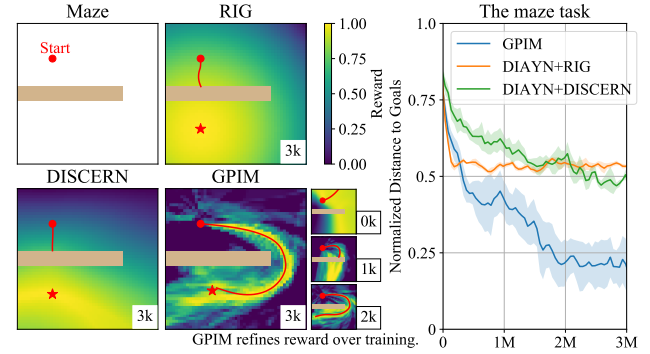


Figure 8. (Left) The maze environment and reward functions. The heatmaps depict the reward function conditioned on the specific task reaching the left-bottom star (RIG and DISCERN) or “imitating” the trajectories (red) induced by abstract-level policy (GPIM). Note that the reward functions of baselines are conditioned on the goals, while GPIM’s reward function is conditioned on the skill ω . So the induced trajectories by GPIM conditioned on the same skill *refines* over training steps, as shown in the bottom. (Right) Learning curves for GPIM and the enhanced baselines (DIAYN+RIG and DIAYN+DISCERN), both of which take r'_t as the reward for generating diverse goals. Compared with our model, the enhanced baselines ignoring the dynamic of the maze environment exhibit poor performance.

environment? Our next experiment studies the expressiveness of the learned reward function. For better graphical interpretation and comparison with baselines, we simplify the complex Atari games to a maze environment shown in Figure 8, where the middle wall poses a bottleneck state. Campos et al. (2020) shows that the canonical information-theoretic skill discovery methods suffer from a poor coverage of the state space. Here, borrowing the idea from state marginal matching (Lee et al., 2019), we set the reward for the abstract-level policy as (Jabri et al., 2019) $r'_t = \lambda [\log q_\phi(\omega|s_{t+1}) - \log p(\omega)] + (\lambda - 1) \log q_\nu(s_{t+1})$, where q_ν is a density model, and $\lambda \in [0, 1]$ can be interpreted as trade off between discriminability of skills and

task-specific exploration (here we set $\lambda = 0.5$). Note that we modify r'_t for improving the exploration on generating goals, and we do not change the reward for training the goal-conditioned policy π_θ . To guarantee generation of the same diverse goals for training goal-conditioned policies of baselines, we adopt DIAYN taking the modified reward r'_t to generate goals for RIG and DISCERN, denoted as DIAYN+RIG and DIAYN+DISCERN respectively.

In Figure 8, we visualize the learned reward on a specific task reaching the left-bottom star, and the learning curves on the maze task, where the testing-goals are random sampled. We can see that the learned reward functions of RIG and DISCERN produce poor signal for the goal-conditioned policy, which makes learning vulnerable to local optima. Our method acquires the reward function after exploring the environment, the dynamic of which itself further shapes the reward function. In Figure 8 (left), we can see that our model provides the reward function better expressiveness of the task by compensating for the dynamic. This produces that, even with the same exploration capability to generate diverse goals, our model sufficiently outperforms the baselines, as shown in Figure 8 (right).

7. Conclusion

We propose GPIM to learn a goal-conditioned policy in an unsupervised manner. Specifically, we optimize a discriminator in an unsupervised manner for the purpose of reliable exploration to provide the intrinsic reward for the abstract-level policy. The learned discriminator then serves as an intrinsic reward function for the goal-conditioned policy to imitate the trajectory induced by the abstract-level policy. Experiments on a variety of robotic tasks demonstrate the effectiveness and efficiency of our proposed method, which substantially outperforms prior unsupervised techniques.

Acknowledgements. The authors gratefully acknowledge funding support from the Westlake University and Bright Dream Joint Institute for Intelligent Robotics.

References

- Achiam, J., Edwards, H., Amodei, D., and Abbeel, P. Variational option discovery algorithms. *arXiv preprint arXiv:1807.10299*, 2018.
- Amodei, D., Olah, C., Steinhardt, J., Christiano, P., Schulman, J., and Mané, D. Concrete problems in ai safety. *arXiv preprint arXiv:1606.06565*, 2016.
- Andrychowicz, M., Wolski, F., Ray, A., Schneider, J., Fong, R., Welinder, P., McGrew, B., Tobin, J., Abbeel, O. P., and Zaremba, W. Hindsight experience replay. In *Advances in neural information processing systems*, pp. 5048–5058, 2017.
- Aubret, A., Matignon, L., and Hassas, S. A survey on intrinsic motivation in reinforcement learning. *arXiv preprint arXiv:1908.06976*, 2019.
- Badia, A. P., Piot, B., Kapturowski, S., Sprechmann, P., Vitvitskyi, A., Guo, D., and Blundell, C. Agent57: Outperforming the atari human benchmark. *arXiv preprint arXiv:2003.13350*, 2020.
- Baranes, A. and Oudeyer, P.-Y. Active learning of inverse models with intrinsically motivated goal exploration in robots. *Robotics and Autonomous Systems*, 61(1):49–73, 2013.
- Barber, D. and Agakov, F. V. The im algorithm: a variational approach to information maximization. In *Advances in neural information processing systems*, pp. None, 2003.
- Beaudry, N. J. and Renner, R. An intuitive proof of the data processing inequality. *arXiv preprint arXiv:1107.0740*, 2011.
- Berner, C., Brockman, G., Chan, B., Cheung, V., Debiak, P., Dennison, C., Farhi, D., Fischer, Q., Hashme, S., Hesse, C., et al. Dota 2 with large scale deep reinforcement learning. *arXiv preprint arXiv:1912.06680*, 2019.
- Brockman, G., Cheung, V., Pettersson, L., Schneider, J., Schulman, J., Tang, J., and Zaremba, W. Openai gym, 2016.
- Burda, Y., Edwards, H., Pathak, D., Storkey, A., Darrell, T., and Efros, A. A. Large-scale study of curiosity-driven learning. *ArXiv*, abs/1808.04355, 2019.
- Campos, V. A., Trott, A., Xiong, C., Socher, R., i Ni-eto, X. G., and Torres, J. Explore, discover and learn: Unsupervised discovery of state-covering skills. *ArXiv*, abs/2002.03647, 2020.
- Co-Reyes, J. D., Liu, Y., Gupta, A., Eysenbach, B., Abbeel, P., and Levine, S. Self-consistent trajectory autoencoder: Hierarchical reinforcement learning with trajectory embeddings. *arXiv preprint arXiv:1806.02813*, 2018.
- Colas, C., Sigaud, O., and Oudeyer, P.-Y. Gep-pg: Decoupling exploration and exploitation in deep reinforcement learning algorithms. *arXiv preprint arXiv:1802.05054*, 2018.
- Colas, C., Karch, T., Lair, N., Dussoux, J.-M., Moulin-Frier, C., Dominey, P. F., and Oudeyer, P.-Y. Language as a cognitive tool to imagine goals in curiosity-driven exploration. *ArXiv*, abs/2002.09253, 2020.
- Eysenbach, B., Gupta, A., Ibarz, J., and Levine, S. Diversity is all you need: Learning skills without a reward function. *arXiv preprint arXiv:1802.06070*, 2018.

- Florensa, C., Degraeve, J., Heess, N., Springenberg, J. T., and Riedmiller, M. Self-supervised learning of image embedding for continuous control. *arXiv preprint arXiv:1901.00943*, 2019.
- Gregor, K., Rezende, D. J., and Wierstra, D. Variational intrinsic control. *arXiv preprint arXiv:1611.07507*, 2016.
- Haarnoja, T., Zhou, A., Abbeel, P., and Levine, S. Soft actor-critic: Off-policy maximum entropy deep reinforcement learning with a stochastic actor. *arXiv preprint arXiv:1801.01290*, 2018.
- Hafner, D., Ortega, P. A., Ba, J., Parr, T., Friston, K., and Heess, N. Action and perception as divergence minimization. *arXiv preprint arXiv:2009.01791*, 2020.
- Hartikainen, K., Geng, X., Haarnoja, T., and Levine, S. Dynamical distance learning for semi-supervised and unsupervised skill discovery. In *International Conference on Learning Representations*, 2019.
- Hausman, K., Springenberg, J. T., Wang, Z., Heess, N., and Riedmiller, M. Learning an embedding space for transferable robot skills. 2018.
- Higgins, I., Matthey, L., Pal, A., Burgess, C., Glorot, X., Botvinick, M., Mohamed, S., and Lerchner, A. beta-vae: Learning basic visual concepts with a constrained variational framework. *Iclr*, 2(5):6, 2017a.
- Higgins, I., Pal, A., Rusu, A., Matthey, L., Burgess, C., Pritzel, A., Botvinick, M., Blundell, C., and Lerchner, A. Darla: Improving zero-shot transfer in reinforcement learning. In *Proceedings of the 34th International Conference on Machine Learning-Volume 70*, pp. 1480–1490. JMLR. org, 2017b.
- Jabri, A., Hsu, K., Gupta, A., Eysenbach, B., Levine, S., and Finn, C. Unsupervised curricula for visual meta-reinforcement learning. In *Advances in Neural Information Processing Systems*, pp. 10519–10531, 2019.
- Khirodkar, R., Yoo, D., and Kitani, K. M. Vadra: Visual adversarial domain randomization and augmentation. *arXiv preprint arXiv:1812.00491*, 2018.
- Kingma, D. P. and Welling, M. Auto-encoding variational bayes. *arXiv preprint arXiv:1312.6114*, 2013.
- Kovač, G., Laversanne-Finot, A., and Oudeyer, P.-Y. Grimgep: learning progress for robust goal sampling in visual deep reinforcement learning. *arXiv preprint arXiv:2008.04388*, 2020.
- Lee, L., Eysenbach, B., Parisotto, E., Xing, E., Levine, S., and Salakhutdinov, R. Efficient exploration via state marginal matching. *arXiv preprint arXiv:1906.05274*, 2019.
- Lee, Y., Sun, S.-H., Somasundaram, S., Hu, E. S., and Lim, J. J. Composing complex skills by learning transition policies. In *International Conference on Learning Representations*, 2018.
- Levine, S., Kumar, A., Tucker, G., and Fu, J. Offline reinforcement learning: Tutorial, review, and perspectives on open problems. *arXiv preprint arXiv:2005.01643*, 2020.
- Levy, A., Konidaris, G., Platt, R., and Saenko, K. Learning multi-level hierarchies with hindsight. *arXiv preprint arXiv:1712.00948*, 2017.
- Lowrey, K., Rajeswaran, A., Kakade, S., Todorov, E., and Mordatch, I. Plan online, learn offline: Efficient learning and exploration via model-based control. *arXiv preprint arXiv:1811.01848*, 2018.
- Nair, A., Bahl, S., Khazatsky, A., Pong, V., Berseth, G., and Levine, S. Contextual imagined goals for self-supervised robotic learning. *arXiv preprint arXiv:1910.11670*, 2019.
- Nair, A. V., Pong, V., Dalal, M., Bahl, S., Lin, S., and Levine, S. Visual reinforcement learning with imagined goals. In *Advances in Neural Information Processing Systems*, pp. 9191–9200, 2018.
- Oudeyer, P.-Y., Kaplan, F., and Hafner, V. V. Intrinsic motivation systems for autonomous mental development. *IEEE transactions on evolutionary computation*, 11(2): 265–286, 2007.
- Pathak, D., Agrawal, P., Efros, A. A., and Darrell, T. Curiosity-driven exploration by self-supervised prediction. *2017 IEEE Conference on Computer Vision and Pattern Recognition Workshops (CVPRW)*, pp. 488–489, 2017.
- Pathak, D., Gandhi, D., and Gupta, A. Self-supervised exploration via disagreement. In *International Conference on Machine Learning*, pp. 5062–5071. PMLR, 2019.
- Péré, A., Forestier, S., Sigaud, O., and Oudeyer, P.-Y. Unsupervised learning of goal spaces for intrinsically motivated goal exploration. *arXiv preprint arXiv:1803.00781*, 2018.
- Pitis, S., Chan, H., Zhao, S., Stadie, B. C., and Ba, J. Maximum entropy gain exploration for long horizon multi-goal reinforcement learning. *ArXiv*, abs/2007.02832, 2020.
- Pong, V., Gu, S., Dalal, M., and Levine, S. Temporal difference models: Model-free deep rl for model-based control. *arXiv preprint arXiv:1802.09081*, 2018.
- Pong, V. H., Dalal, M., Lin, S., Nair, A., Bahl, S., and Levine, S. Skew-fit: State-covering self-supervised reinforcement learning. *arXiv preprint arXiv:1903.03698*, 2019.

- Popov, I., Heess, N., Lillicrap, T., Hafner, R., Barth-Maron, G., Vecerik, M., Lampe, T., Tassa, Y., Erez, T., and Riedmiller, M. Data-efficient deep reinforcement learning for dexterous manipulation. *arXiv preprint arXiv:1704.03073*, 2017.
- Puterman, M. L. *Markov decision processes: discrete stochastic dynamic programming*. John Wiley & Sons, 2014.
- Salge, C., Glackin, C., and Polani, D. Empowerment—an introduction. In *Guided Self-Organization: Inception*, pp. 67–114. Springer, 2014.
- Schaul, T., Horgan, D., Gregor, K., and Silver, D. Universal value function approximators. In *International conference on machine learning*, pp. 1312–1320, 2015.
- Schulman, J., Wolski, F., Dhariwal, P., Radford, A., and Klimov, O. Proximal policy optimization algorithms. *arXiv preprint arXiv:1707.06347*, 2017.
- Sermanet, P., Lynch, C., Chebotar, Y., Hsu, J., Jang, E., Schaal, S., Levine, S., and Brain, G. Time-contrastive networks: Self-supervised learning from video. In *2018 IEEE International Conference on Robotics and Automation (ICRA)*, pp. 1134–1141. IEEE, 2018.
- Sharma, A., Gu, S., Levine, S., Kumar, V., and Hausman, K. Dynamics-aware unsupervised discovery of skills. *arXiv preprint arXiv:1907.01657*, 2019.
- Srinivas, A., Laskin, M., and Abbeel, P. Curl: Contrastive unsupervised representations for reinforcement learning. *arXiv preprint arXiv:2004.04136*, 2020.
- Still, S. and Precup, D. An information-theoretic approach to curiosity-driven reinforcement learning. *Theory in Biosciences*, 131:139–148, 2011.
- Sukhbaatar, S., Lin, Z., Kostrikov, I., Synnaeve, G., Szlam, A., and Fergus, R. Intrinsic motivation and automatic curricula via asymmetric self-play. *arXiv preprint arXiv:1703.05407*, 2017.
- Sukhbaatar, S., Denton, E., Szlam, A., and Fergus, R. Learning goal embeddings via self-play for hierarchical reinforcement learning. *arXiv preprint arXiv:1811.09083*, 2018.
- Sutton, R. S. and Barto, A. G. *Reinforcement learning: An introduction*. MIT press, 2018.
- Tanwani, A. K. Domain-invariant representation learning for sim-to-real transfer. *arXiv preprint arXiv:2011.07589*, 2020.
- Tian, Q., Liu, J., and Wang, D. Learning transitional skills with intrinsic motivation, 2020. URL <https://openreview.net/forum?id=ryeRwlSYPH>.
- Tobin, J., Fong, R., Ray, A., Schneider, J., Zaremba, W., and Abbeel, P. Domain randomization for transferring deep neural networks from simulation to the real world. In *2017 IEEE/RSJ International Conference on Intelligent Robots and Systems (IROS)*, pp. 23–30. IEEE, 2017.
- Vecerik, M., Sushkov, O., Barker, D., Rothörl, T., Hester, T., and Scholz, J. A practical approach to insertion with variable socket position using deep reinforcement learning. In *2019 International Conference on Robotics and Automation (ICRA)*, pp. 754–760. IEEE, 2019.
- Wardle-Farley, D., de Wiele, T. V., Kulkarni, T. D., Ionescu, C., Hansen, S., and Mnih, V. Unsupervised control through non-parametric discriminative rewards. In *7th International Conference on Learning Representations, ICLR 2019, New Orleans, LA, USA, May 6-9, 2019*. OpenReview.net, 2019. URL <https://openreview.net/forum?id=r1eVMnA9K7>.
- Watter, M., Springenberg, J., Boedecker, J., and Riedmiller, M. Embed to control: A locally linear latent dynamics model for control from raw images. In *Advances in neural information processing systems*, pp. 2746–2754, 2015.
- Xu, G., Liu, Z., Li, X., and Loy, C. C. Knowledge distillation meets self-supervision. *arXiv preprint arXiv:2006.07114*, 2020.
- Zhang, R., Isola, P., Efros, A. A., Shechtman, E., and Wang, O. The unreasonable effectiveness of deep features as a perceptual metric. In *Proceedings of the IEEE Conference on Computer Vision and Pattern Recognition*, pp. 586–595, 2018.

A. Additional Experiments

A.1. Comparison with DIAYN and its Variant

In this section, we expect to clarify the difference and connection with DIAYN (Eysenbach et al., 2018) experimentally, and indicate the limitations of maximizing $\mathcal{I}(s; \omega)$ and maximizing $\mathcal{I}(s; g)$ separately on learning goal-conditioned policy.

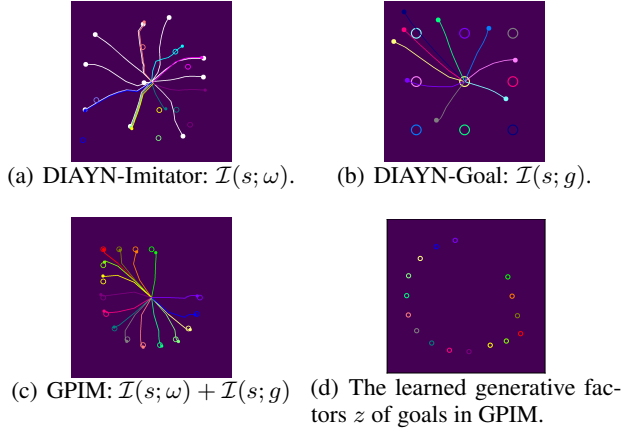


Figure 9. 2D navigation with (a) DIAYN-Imitator, (b) DIAYN-Goal, and (c) our proposed GPIM. In (a), (b) and (c), the open circle denotes the user-specified goal, and the line with a solid circle at the end is the corresponding behavior. Specifically, the white lines in (a) are the learned skills in training, where we show 10 diverse skills. We can see that neither DIAYN-Imitator nor DIAYN-Goal approaches the corresponding goals, while our model succeeds in reaching the goal as shown in (c). In (d), we also show the generative factors z (see Figure 2 in section A.2) by disentangling goals with the regularization loss in (d), where the open circles with different colors in (c) correspond to the goals in (d).

In DIAYN, authors show the ability of the model to imitate an expert. Given the goal, DIAYN uses the learned discriminator to estimate which skill was most likely to have generated the goal g :

$$\hat{\omega} = \arg \max_{\omega} q_{\phi}(\omega|g). \quad (8)$$

Here we call this model *DIAYN-Imitator*. We also directly substitute the perceptually-specific goals for the latent variable in DIAYN’s objective to learn a goal-conditioned policy. We call this model *DIAYN-Goal*:

$$\max \mathcal{I}(s; g), \quad (9)$$

where g is sampled from the prior goal distribution $p(g)$. Please note that we do not adopt the prior non-parametric distance as in DISCERN (Warde-Farley et al., 2019) to calculate the reward. We obtain the reward as in normal DIAYN using the variational inference: $r_t = q_{\phi}(g_t|s_{t+1})$.

Figure 9 shows the comparison of our GPIM with DIAYN variants including DIAYN-Imitator and DIAYN-Goal, where the 2D navigation task is considered. As observed, DIAYN-Imitator can reach seen goals but not unseen goals in Figure 9(a), because it cannot effectively accomplish the interpolation between skills that are induced in training. And behaviors generated by DIAYN-Goal cannot guarantee consistency with the preset goals in Figure 9(b). The main reason is that this objective only ensures that when g (or ω) is different, the states generated by g (or ω) are different. However, there is no guarantee that g (or ω) and the state generated by the current g (or ω) have semantically consistent behavior information. Our proposed GPIM method, capable of solving interpolation and consistency issues, exhibits the best performance in this 2D navigation task.

Moreover, when the user-specified goals are heterogeneous to the states, the learned discriminator q_{ϕ} in DIAYN is unable to estimate which skill is capable of inducing given goals. Specifically, when the goals are visual inputs, and the states in training is feature vectors (e.g., joint angles), the learned discriminator is unable to choose the skills due to a lack of models for converting high-dimensional figure into low-dimensional feature vectors. On the contrary, there are lots of off-the-shelf models to render low-dimensional feature vectors into perceptually-specific high-dimensional inputs (Tobin et al., 2017; Khironkar et al., 2018).

A.2. Implementing π_{θ} with Latent Variable Models

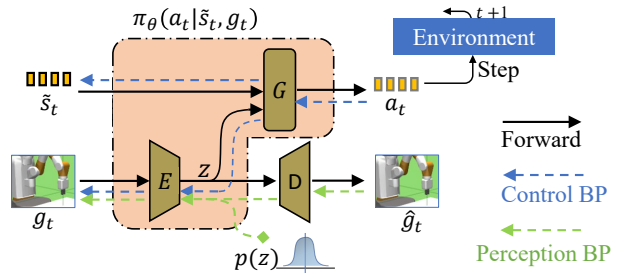


Figure 10. Optimization for the goal-conditioned policy π_{θ} with the control-level loss (SAC with reward \tilde{r}_t) and perception-level loss.

As indicated by Srinivas et al. (2020), control algorithms built on top of useful semantic representations should be significantly more data-efficient. We further optimize the goal-conditioned policy π_{θ} with an associated regularization loss on the perception level, so as to improve the learning efficiency and generalization ability of the goal-conditioned policy π_{θ} facing high-dimensional goals. As shown in Figure 10, we decompose π_{θ} into two components: the encoder network E parameterized by ϑ_E and the generative network G parameterized by ϑ_G . Hence, we optimize the overall

objective function for the goal-conditioned policy π_θ :

$$\max_{\vartheta_E, \vartheta_G, \vartheta_D} \mathbb{E}_{\omega, \tilde{s}_t} [\tilde{r}_t] + \text{Prec_loss}, \quad (10)$$

where the regularization loss on the perception level Prec_loss includes the reconstruction loss and a prior matching loss (with an isotropic unit Gaussian prior $p(z) = N(0; I)$):

$$\underbrace{\alpha \cdot \mathbb{E}_{g_t, z} [p_{\vartheta_D}(g_t|z)]}_{\text{reconstruction loss}} - \underbrace{\beta \cdot \mathbb{E}_{g_t} [KL(q_{\vartheta_E}(z|g_t)||p(z))]}_{\text{prior matching loss}},$$

α and β are two hyperparameters. It is worth noting that the update of the encoder E is based on gradients from both π_θ and Prec_loss .

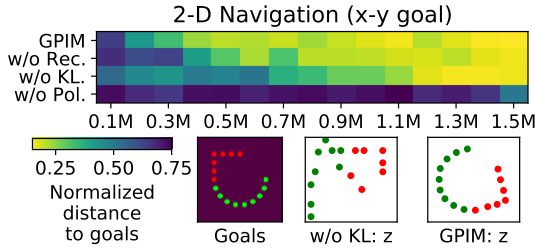


Figure 11. Ablation study for the perception loss.

Ablation study on 2D navigation. Here we conduct the ablation study on 2D navigation task to analyze how the regularization loss in GPIM affects the learned behaviors in terms of the generalization to new tasks. For convenience, we remove certain component from GPIM and define the new method as follows: *w/o Rec* - removing the reconstruction loss (i.e. $\alpha = 0$); *w/o KL* - removing the KL loss (i.e. $\beta = 0$); *w/o Pol* - removing the policy loss updating ϑ_E as shown in Figure 10.

The performance is reported in Figure 11. It is observed that *w/o. Pol* performs worse than all other methods, which is consistent with the performance of RIG that trains VAE and policy separately. The main reason is that the regularization loss fails to figure out the required latent factors on given tasks. Moreover, although GPIM has a similar performance with the other three methods on 2D navigation task, GPIM has better interpretability to behaviors. As shown at the bottom of Figure 11, considering a series of goals from the first red to the last green (left) in a counterclockwise order, GPIM can successfully disentangle them and learn effective latent z (right), but *w/o KL* fails to keep the original order of goals (middle).

Ablation study on mujoco tasks. We further study the impact of regularization loss on mujoco tasks. The performance is reported in Figure 12. It is observed that *w/o Pol* performs worse than all other methods, which is consistent

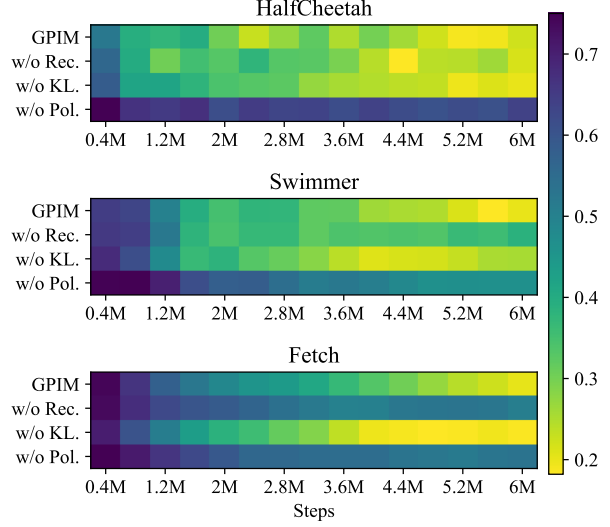


Figure 12. Ablation study on mujoco tasks (half cheetah, swimmer and fetch): the normalized distance to goals vs. the training steps.

with the performance in 2D navigation task⁶. And we can find that when we remove the reconstruction loss ($\alpha = 0$), the performance of *w/o Rec* degrades in these three environments. The main reason is that the process of learning generative factors become more difficult without the supervised reconstruction loss. While in 2D navigation task, the reconstruction loss has little impact on the performance. Even though that *w/o KL* has a similar performance with our full GPIM method, GPIM demonstrates better interpretability to behaviors as shown in Figure 9(d).

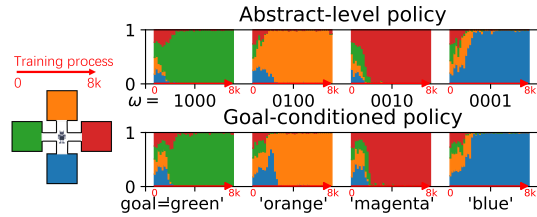


Figure 13. Gridworld tasks. Y-axis is the percentage of different rooms that the robot arrives in.

A.3. Generalization on the Gridworld Task

Here we introduce an illustrative example of gridworld task and then show the generalization when the dynamics and goal conditions are missing in the gridworld task.

Illustrative example. Here, we start with a simple gridworld example: the environment is shown on the left of Figure 13, where the goal for the agent is to navigate from the middle to the given colored room. By abstract-level

⁶The results of 2D navigation task are shown in the full paper.

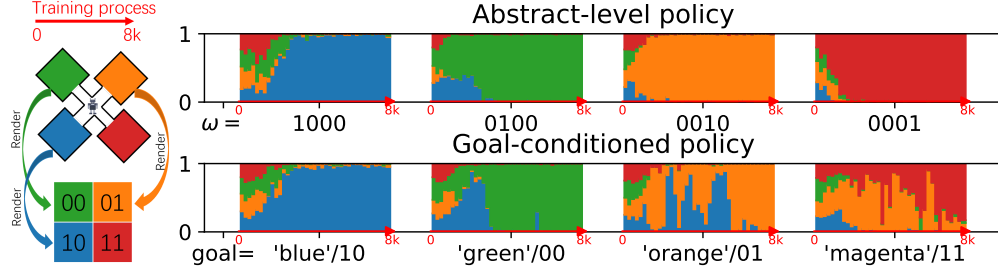


Figure 14. Gridworld tasks. The Y-axis is the percentage of different rooms that agent arrives in.

training, our method quickly acquire four skills to reach different rooms. Each time the agent arrives in a room induced by π_μ , we train π_θ conditioned on the room’s color (e.g., green), allowing the agent to be guided to the same room by the current reward function. The learning process is shown on the right of Figure 13. It is concluded that the agent can automatically learn how to complete tasks given semantic goals in an unsupervised manner.

Generalization on the gridworld task. We further show the generalization when the dynamics and goal conditions are missing in the gridworld task, where there are four rooms in different colors: blue, green, orange and magenta. We consider the situation where we train the goal-conditioned policy in the blue room, the green room and the orange room, and test in the magenta room.

As shown in Figure 14, we quickly acquire four skills for different rooms through the training at the abstract level. After the agent reaches at the colored rooms, we rendered the corresponding room as a two-bit representation: $\text{Render}(\text{'blue'}) = 10$, $\text{Render}(\text{'green'}) = 00$, and $\text{Render}(\text{'orange'}) = 01$; we do not render the magenta room. We take the magenta room corresponding to 11 as the test goal to verify the generalization ability.

In lower part of Figure 14, we show the learning process of the goal-conditioned policy. We can find that the blue room tasks are learned quickly, and the green and magenta room tasks are learned relatively slowly, but the agent is still able to complete the test task successfully (the magenta room). Compared to the task in Figure 13 that renders all the rooms as goals, the whole learning process in Figure 14 is much slower. We hypothesize that the main reason is that the agent needs to further infer the relationship between different goals. The lack of goal information (i.e., missing magenta 11) leads to a lower efficiency and unstable training.

A.4. Automated Goal-Generation for Exploration

In general, for unsupervised RL, we would like to ask the agent to carry out autonomous “practice” during training phase, where we do not know which particular goals will be provided in test phase. In order to maximize the state cov-

erage, the ability to automatically explore the environment and discover diverse goals is crucial. In this section, we will further analyze the goal distribution of three methods (RIG (Nair et al., 2018), DISCERN (Warde-Farley et al., 2019), GPIM) in a new 2D obstacle navigation task as shown in Figure 15(a), Figure 15(b), and Figure 15(c). The size of the environment is 10×10 , the initial state is set as $[5, 2]$, and there are two obstacles that prevent the agent from passing through each of which is 3×6 in size.

DISCERN samples goals during training by maintaining a fixed sized buffer \mathcal{G} of past observations. We simply mimic the process of goal generation by taking random actions for 20 environment steps after initialization of the method. As in Figure 15(b), we generate 100 goals with different colors. We can see that the majority of goals locate between the two obstacles, which limits the further exploration of the environment.

RIG samples a representation (latent goals z_g) from the learned VAE prior, which represents a distribution over latent goals and state observation. The policy network takes the representation as a substitute for the user-specified goal. For a clear visualization of the distribution of the sampled latent goals, we further feed the sampled latent goals into the decoder to obtain the real goals in the user-specified space. The decoded latent goals are shown in Figure 15(a), where we sample 30 goals. It is shown that the majority of goals are also between the two obstacles because the goals for training the VAE prior come from the same distribution as in DISCERN.

Our method, GPIM, obtains goals from the behaviors induced by the abstract-level policy. Maximizing $\mathcal{I}(s; \omega)$ encourages different skills to induce different states that are further rendered to goals. This objective ensures that each skill individually is distinct and the skills collectively explore large parts of the state space (Eysenbach et al., 2018). As shown in Figure 15(c), our method provides better coverage of the state space than DISCERN and RIG.

Figure 15(d) shows the performance of the three methods, where we randomly sample goals from the whole state (or goal) space at test phase. We can see that our method signifi-

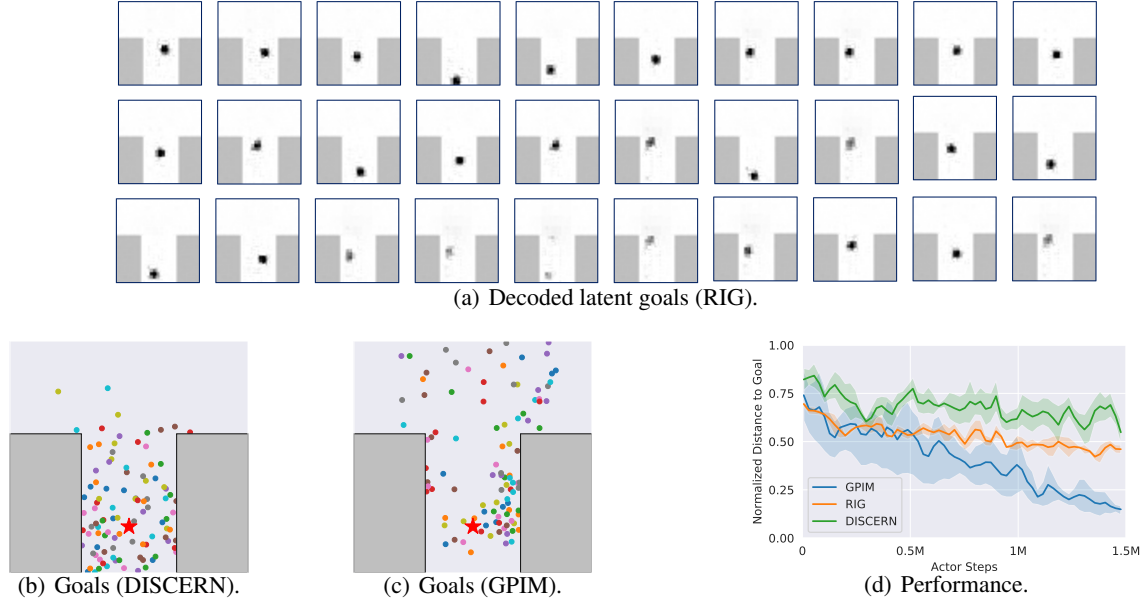


Figure 15. Distribution of sampled goals for the goal-conditioned policy, where the initial state is [5,2] (the red star) and the actor step is 20 for each rollout. (a) The goals (images) are obtained by decoding 30 sampled latent goals z_g in VAE framework; (b) The goals (colored dots) are sampled from the agent’s behaviors by random exploration; (c) The goals (colored dots) are rendered from the states induced by our abstract-level policy. (d): Evaluation on reaching user-specified goals, where GPIM significantly outperforms baselines.

cantly outperforms the baselines. The most common failure mode for prior methods is that the goal distribution collapses (Pong et al., 2019), causing that the agent can reach only a fraction of the state space, as shown in Figure 15(a) and 15(b).

Exploration is a well-studied problem in the field of RL, and there are many proven approaches with different benefits to improve the exploration (Colas et al., 2018; Campos et al., 2020). Note that these benefits are orthogonal to those provided by our straightforward GPIM, and these approaches could be combined with GPIM for even greater effect. We leave combining our method with sophisticated exploration strategies to future work.

B. Derivation

B.1. Derivation of the Variational Bound

$$\begin{aligned}
 & \mathbb{E}_{p_m(\cdot)} [\log p(\omega|s) + \log p(\omega|\tilde{s}) - 2 \log p(\omega)] \\
 = & \mathbb{E}_{p_m(\cdot)} [\log q_\phi(\omega|s) + \log q_\phi(\omega|\tilde{s}) - 2 \log p(\omega)] \\
 & + KL(p(\omega|s) || q_\phi(\omega|s)) + KL(p(\omega|\tilde{s}) || q_\phi(\omega|\tilde{s})) \\
 \geq & \mathbb{E}_{p_m(\cdot)} [\log q_\phi(\omega|s) + \log q_\phi(\omega|\tilde{s}) - 2 \log p(\omega)]
 \end{aligned}$$

B.2. Proof of Theoretical Guarantees

Note that $\eta(\pi_\theta) = \mathbb{E}_{p(g, \tilde{s}; \theta)} [\log p(g|\tilde{s}) - \log p(g)]$, and $\hat{\eta}(\pi_\theta) = \mathbb{E}_{p(\omega, s, g, \tilde{s}; \mu, \kappa, \theta)} [\log p(\omega|\tilde{s}) - \log p(\omega)]$ subject to

$\mathcal{I}(\omega; s) \geq C$. We characterize the relationship between the two objectives:

$$\begin{aligned}
 & \hat{\eta}(\pi_\theta) - \eta(\pi_\theta) \quad \# p_m(\cdot) \triangleq p(\omega, s, g, \tilde{s}; \mu, \kappa, \theta) \\
 = & \mathbb{E}_{p_m(\cdot)} [\log p(\omega|\tilde{s}) - \log p(\omega)] - \mathbb{E}_{p(g, \tilde{s}; \theta)} [\log p(g|\tilde{s}) - \log p(g)] \\
 = & \underbrace{\mathbb{E}_{p_m(\cdot)} [\log p(\omega|\tilde{s}) - \log p(\omega) - \log p(g|\tilde{s}) + \log p(g)]}_{\text{TERM-I}} \\
 & + \underbrace{\mathbb{E}_{p_m(\cdot)} [\log p(g|\tilde{s}) - \log p(g)] - \mathbb{E}_{p(g, \tilde{s}; \theta)} [\log p(g|\tilde{s}) - \log p(g)]}_{\text{TERM-II}}.
 \end{aligned}$$

If we assume the prior goal distribution $p(g)$ for optimizing $\eta(\pi_\theta)$ matches the goal distribution $p(g|\omega; \mu, \kappa)$ induced by π_μ and render κ for optimizing $\hat{\eta}(\pi_\theta)$, eg $p_m(\cdot) = p(\omega, s; \mu)p(g, \tilde{s}; \theta)$, we obtain TERM-II = 0 and TERM-I = $\mathbb{E}_{p(\omega, s, g; \mu, \kappa)} [\log p(s|\omega; \mu) + \log p(g|s; \kappa)]$. If $p_m(\cdot) \triangleq p(\omega, s; \mu)p(g, \tilde{s}|\omega, s; \kappa, \theta) \neq p(\omega, s; \mu)p(g, \tilde{s}; \theta)$, we apply Holder’s inequality and Pinsker’s inequality over TERM-II. Then the following inequality holds:

$$\begin{aligned}
 & \text{TERM-II} \\
 = & \mathbb{E}_{p(\omega, s; \mu)} [\mathbb{E}_{p(g, \tilde{s}|\omega, s; \kappa, \theta)} [R(g, \tilde{s})] - \mathbb{E}_{p(g, \tilde{s}; \theta)} [R(g, \tilde{s})]] \\
 \leq & \mathbb{E}_{p(\omega, s; \mu)} [\|R(g, \tilde{s})\|_\infty \cdot \|p(g, \tilde{s}|\omega, s; \kappa, \theta) - p(g, \tilde{s}; \theta)\|_1] \\
 \leq & \mathbb{E}_{p(\omega, s; \mu)} \left[\left(\max_{g, \tilde{s}} R(g, \tilde{s}) \right) \cdot 2 \sqrt{\frac{1}{2} D_{\text{KL}}(p(g, s|\omega, s; \kappa, \theta) || p(g, s; \theta))} \right],
 \end{aligned}$$

where $R(g, \tilde{s}) = \log p(g|\tilde{s}) - \log p(g)$.

C. Implementation Details

C.1. Environment Details

We introduce the details of environments and tasks here, including the environment setting of 2D navigation (*x-y goal* and *color-shape goal*), object manipulation, three atari games (seaquest, berzerk and montezuma revenge), and the mujoco tasks (swimmer, half cheetah and fetch).

2D navigation tasks: In 2D navigation tasks, the agent moves in each of the four cardinal directions, where the states denote the 2D location of the agent. We consider the following two tasks: moving the agent to a specific coordinate named *x-y goal* and moving the agent to a specific object with certain color and shape named *color-shape goal*.

- **2D Navigation (*x-y goal*):** The size of the environment is 10×10 (continuous state space) or 7×7 (discrete state space). The state is the location of the agent, and the goal is the location of the final location.
- **2D Navigation (*color-shape goal*):** The size of the environment is 10×10 . The state consists of the locations of the agent and three objects with different color-shape pairs (one real target and two distractors). The goal is described by the color and shape of the real target, encoded with one-hot.

Object manipulation: More complex manipulation considers a moving agent in 2D environment with one block for manipulation, and the other as a distractor. The agent first needs to reach the block and then move the block to the given location, where the block is described using color and shape. The size of the environment is 10×10 . The state consists of the locations of the agent and two blocks with different color-shape pairs (one real target and one distractor). The goal consists of the one-hot encoding of the color-shape of the target block that needs to be moved, and the 2D coordinate of the final location of the movement.

Table 1. The repetition length of the action.

Environments	k
Seaquest-ram-v0	2, 3, 4, 5
Berzerk-ram-v0	34, 36, 38, 40
MontezumaRevenge-ram-v0	2, 3, 4, 5

Atari games: We test the performance on three atari games: seaquest, berzerk, and montezuma revenge. In order to reduce the difficulty of training, we adopt the RAM-environment (i.e., Seaquest-ram-v0, Berzerk-ram-v0, and MontezumaRevenge-ram-v0), where each state represents a 128-dimensional vector. Each action repeatedly performs for a duration of k frames, where k is uniformly sampled from Table 1.

Mujoco tasks: We consider to make diverse agents to fast imitate a given goal trajectory, including the imitation of behaviors of a swimmer, a half cheetah, and a fetch, where the states in the trajectory denote the positions of agents. Such experiments are conducted to demonstrate the effectiveness of our proposed method in learning behaviors over a continuous high-dimensional action space, which is more complicated in physics than the 2D navigation.

Note that the goals in all the experiments are images $50 \times 50 \times 3$ (3 channels, RGB) in size, except that the *color-shape goal* is encoded with one-hot.

C.2. Metrics, Network Architectures and Hyperparameters

Here we give a clear definition of our evaluation metric – "normalized distance to goal":

I: When the goal is to reach the final state of the trajectory induced by π_μ (Figs.4 (a), (b), (c)), the distance to goal is the L2-distance between the final state \tilde{s}_{T-1}^k induced by $\pi_\theta(\cdot|\cdot, g^k)$ and the goal state g^k randomly sampled from the goal (task) space:

$$Dis = \frac{1}{N} \sum_{k=1}^N L2(\tilde{s}_{T-1}^k, g^k),$$

where N is the number of testing samples. We set $N = 50$ for 2D navigation, object manipulation and atari games (seaquest, berzerk and montezuma revenge).

II: When the goal is to imitate the whole trajectory induced by π_μ (Figs. (d), (e), (f)), the distance is the expectation of distance over the whole trajectory $\{\tilde{s}_0^k, \tilde{s}_1^k, \dots, \tilde{s}_{T-1}^k\}$ induced by $\pi_\theta(\cdot|\cdot, \{g_0^k, g_1^k, \dots, g_{T-1}^k\})$ and goal trajectory $\{g_0^k, g_1^k, \dots, g_{T-1}^k\}$ randomly sampled from the trajectory (task) space:

$$Dis = \frac{1}{N} \sum_{k=1}^N \left(\frac{1}{T} \sum_{t=0}^{T-1} L2(\tilde{s}_t^k, g_t^k) \right),$$

where N is the number of testing samples. We set $N = 50$ for mujoco tasks (swimmer, half cheetah and fetch).

The term "normalized" means that the distance is divided by a scale factor.

Note that, for three atari games (seaquest, berzerk, and montezuma revenge), the L2-distance for evaluation⁷ is the difference between the position of controllable agent and the target's position, where the position is obtained by matching the pixel on the imaged state.

⁷The reward function for our baseline **L2 Distance** still calculates the L2-distance directly on the original state space, instead of the distance of the agents' positions after pixel matching here.

In our implementation, we use two independent SAC architectures (Haarnoja et al., 2018) for abstract-level policy π_μ and goal-conditioned policy π_θ . We find empirically that having two networks share a portion of the network structure will degrade the experimental performance. We adopt universal value function approximates (UVFAs) (Schaul et al., 2015) for extra input (goals). For the abstract-level policy π_μ , to pass latent variable ω to the Q function, value function, and policy, as in DIAYN, we simply concatenate ω with the current state s_t (and action a_t). For goal-conditioned policy π_θ , we also concatenate g_t with current state \tilde{s}_t (and action a_t). We update the ϑ_E using the gradients from both the *Dis Loss* and Q function’s loss of the goal-conditioned policy π_θ .

The hyper-parameters are presented in Table 2.

D. Broader Impact

The main concern in the research area of goal-conditioned policy is how to find numerous diverse goals as well as obtain the reward function. Particularly, in practical application, the goal and state are often heterogeneous data with high variability of data types and formats, which further aggravates the difficulty of policy learning. Our model addresses these problems by allowing agents to interact with objects or environment, and learn the behaviors in a fully autonomous way on the basis of intrinsic motivations. Bridging with the render function between abstract level and goal-conditioned policy, we could obtain diverse and versatile policies. By optimizing the intrinsic reward, our GPIM makes an agent capable of solving diverse tasks, which fits for wide-range applications such as quick imitation on behavior states, interactive navigation and object manipulation, and so on.

Moreover, our model provides an approach to address the Robot open-Ended Autonomous Learning (REAL). This framework is likely to speed up the progress of the general-purpose robots that can achieve complex tasks given the corresponding goals, and drive the development of autonomous robot learning in a life-long learning mode.

By autonomous exploration of the environment, the agent is likely to generate some useful behaviors as well as the majority of useless skills. Of particular concern is that the use of autonomous exploration is likely to generate a strategy that will induce dire consequences, such as a collision skill in an autonomous driving environment. How to generate useful behaviors for user-specified tasks and how to use these induced skills are also open problems. An alternative solution is to use an extrinsic reward to guide the exploration or the offline reinforcement learning (Levine et al., 2020). While another issue comes from the exploration-exploitation trade-off. We would encourage further work to understand

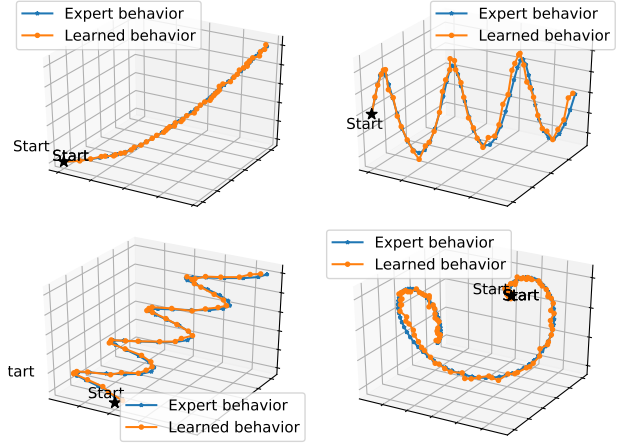


Figure 16. Expert behaviors and learned behaviors. The four expert trajectories are described parametrically as: $(x, y, z) = (\log_{10}(t+1) + t/50, \sin(t)/5 + t/5, t/5)$, $(x, y, z) = (t/5, \cos(t)/5 - 1/5 + t/5, \sin(t)/5)$, $(x, y, z) = (\cos(t)/5 + t/50 - 1/1, \sin(t)/5 + t/5, t/5)$, and $(x, y, z) = (\sin(t) - \sin(2t)/2, -t/5, \cos(t)/2 - \cos(2t)/2)$.

the limitations of REAL interacting with the environment autonomously. We would also encourage research to understand the risks arising from autonomous robot learning.

Another limitation is that our learning framework needs an extra abstract-level policy training for rendering goals and providing a reward function. This requires twice as much interaction time with the environment as learning a single policy network. For practical application, a simulation platform is preferred for pre-training. We also encourage researchers to mitigate the difference between the simulation platform and the actual environment. We also pursue the effective models of transfer learning.

E. More Results

E.1. Learned Behaviors on temporally-extended tasks

More experimental results are given in Figure 16 to show the imitation on several temporally-extended tasks.

E.2. Learned Behaviors from GPIM

More experimental results are given in Figure 17 to show the learned behaviors on 2D navigation, object manipulation, three atari games (seaquest, berzerk and montezuma revenge), and the mujoco tasks (swimmer, half cheetah and fetch). Videos are available under <https://sites.google.com/view/gpim>.

Table 2. Hyper-parameters

Hyper-parameter			value
	Batch Size		256
	Discount Factor		0.99
	Buffer Size		10000
	Smooth coefficient		0.05
	Temperature		0.2
Learning Rate	2D Navigation	x-y goal	0.001
		color-shape goal	0.001
	Object Manipulation		0.001
	Mujoco tasks	Swimmer	0.0001
		HalfCheetah	0.0001
		Fetch	0.0001
	Atari games	Seaquest	0.0003
		Berzerk	0.0003
		Montezuma Revenge	0.0003
Path Length	2D Navigation	x-y goal	20
		color-shape goal	20
	Object Manipulation		20
	Mujoco tasks	Swimmer	50
		HalfCheetah	50
		Fetch	100
	Atari games	Seaquest	25
		Berzerk	25
		Montezuma Revenge	25
Hidden Size	2D Navigation	x-y goal	128
		color-shape goal	128
	Object Manipulation		128
	Mujoco tasks	Swimmer	256
		HalfCheetah	256
		Fetch	256
	Atari games	Seaquest	256
		Berzerk	256
		Montezuma Revenge	256
Dimension of Generative Factor	2D Navigation	x-y goal	2
		color-shape goal	2
	Object Manipulation		4
	Mujoco tasks	Swimmer	3
		HalfCheetah	4
		Fetch	4
	Atari games	Seaquest	16
		Berzerk	16
		Montezuma Revenge	16
α			1
γ			5
δ_{pixel}			255

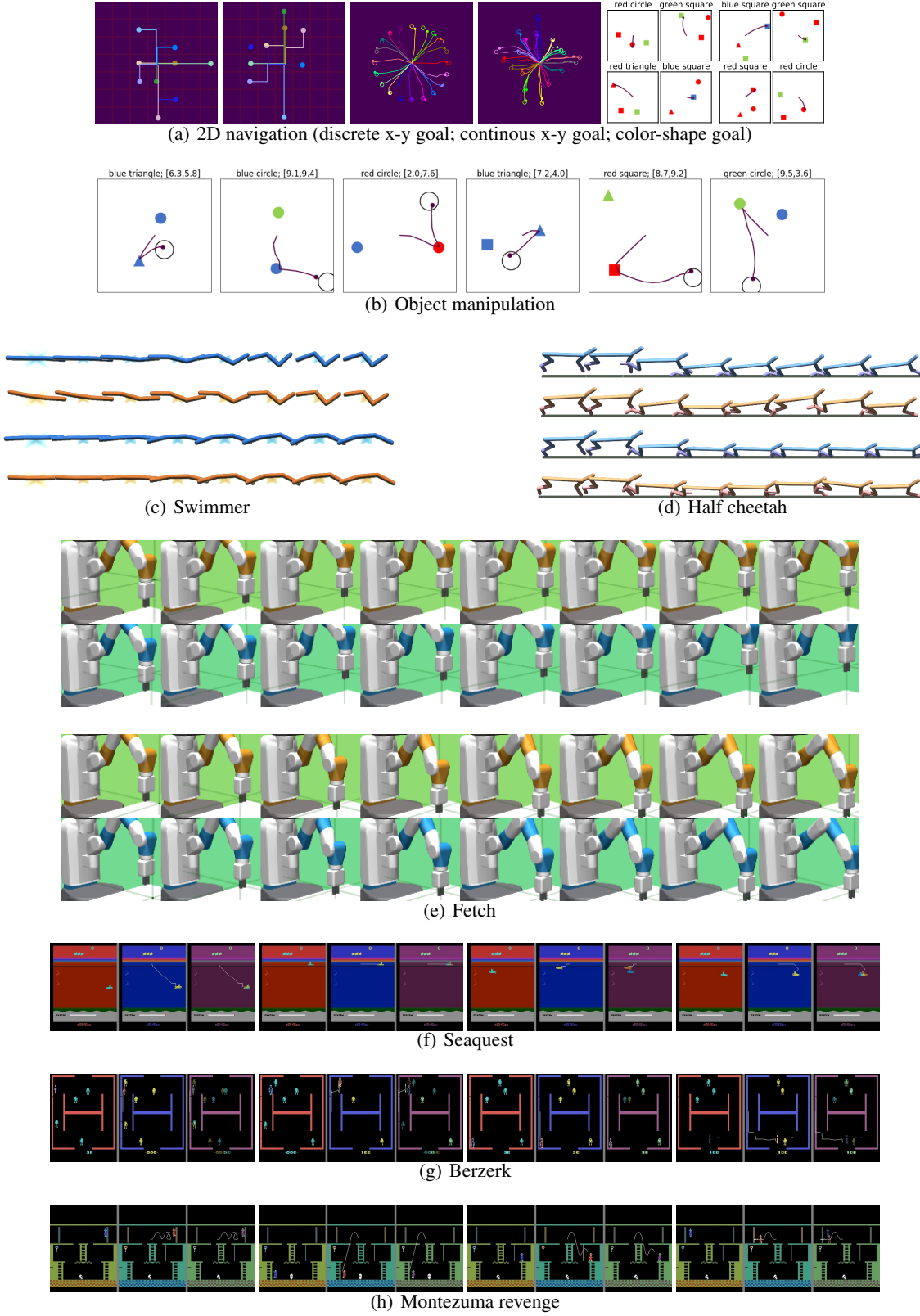


Figure 17. Discovered goal-conditioned behaviors. (f-h): The left subfigure shows the expert behaviors (goals); The middle subfigure shows the learned behaviors by GPIM; The right subfigure is the stacked view of goals and GPIM behaviors.